Atmos. Meas. Tech. Discuss., 2, 781–824, 2009
www.atmos-meas-tech-discuss.net/2/781/2009/

Atmospheric Measurement Techniques Discussions

Atmospheric Measurement Techniques Discussions is the access reviewed discussion forum of *Atmospheric Measurement Techniques*

An improved tropospheric NO_2 retrieval for satellite observations in the vicinity of mountainous terrain

Y. Zhou[1], D. Brunner[1], K. F. Boersma[2], R. Dirksen[2], and P. Wang[2]

[1]Empa, Swiss Federal Lab. for Materials Testing and Research, Dübendorf, Switzerland
[2]Royal Netherlands Meteorological Institute, KNMI, De Bilt, The Netherlands

Received: 4 March 2009 – Accepted: 5 March 2009 – Published: 10 March 2009

Correspondence to: D. Brunner (dominik.brunner@empa.ch)

Published by Copernicus Publications on behalf of the European Geosciences Union.

Abstract

We present an approach to reduce topography-related errors of vertical tropospheric columns (VTC) of NO_2 retrieved from the Ozone Monitoring Instrument (OMI) in the vicinity of mountainous terrain. This is crucial for reliable estimates of air pollution levels over our particular area of interest, the Alpine region and the adjacent planes, where the operational OMI products exhibit significant biases due to the coarse resolution of surface parameters used in the retrieval. Our approach replaces the coarse-gridded surface pressures by accurate pixel-average values using a high-resolution topography data set, and scales the a priori NO_2 profiles accordingly. NO_2 VTC reprocessed in this way for the period 2006–2007 suggest that the current Dutch OMI NO_2 product (DOMINO) underestimates NO_2 over the Po Valley in Italy and over the Swiss plateau by about 20% in winter and 5% in summer under clear-sky conditions (cloud radiance fraction <0.5). A sensitivity analysis shows that these seasonal differences are mainly due to the different a priori NO_2 profile shapes and solar zenith angles in winter and summer. The comparison of NO_2 columns from the original and the enhanced retrieval with corresponding columns deduced from ground-based in situ observations over the Swiss plateau and the Po Valley illustrates the promise of our new retrieval. It partially reduces the underestimation of the OMI VTCs at polluted sites in winter and fall and generally improves the agreement in terms of slope and correlation at rural stations. It does not solve, however, the issue that the OMI DOMINO product tends to overestimate very low columns observed at rural sites in spring and summer.

1 Introduction

Nitrogen dioxide (NO_2) is an important air pollutant affecting human health and ecosystems and playing a major role in the production of tropospheric ozone (Seinfeld and Pandis, 1998; Finlayson-Pitts, 2000). Nitrogen oxides (NO_x=NO+NO_2) have both substantial anthropogenic sources due to combustion of fossil fuels and human-induced biomass burning, and natural sources such as microbial production in soils, wildfires, and lightning. NO_x concentrations exhibit large spatial gradients due to the inhomogeneous distribution of sources and the relatively short lifetime of NO_x in the planetary boundary layer. Observations at high spatial resolution are therefore crucial to reliably assess exposure levels and corresponding environmental impacts.

Complementary to ground-based monitoring networks, which provide detailed information of local near-surface air pollution, satellite remote sensing can extend the spatial coverage and provide area-wide data of NO_2 vertical tropospheric column densities (VTCs). Satellite observations of tropospheric NO_2 using UV/VIS spectrometers began in 1995 with the Global Ozone Monitoring Experiment (GOME) (Burrows et al., 1999), followed by the Scanning Imaging Absorption spectrometer for Atmospheric Chartography (SCIAMACHY) (Bovensmann et al., 1999), the Ozone Monitoring Instrument (OMI) (Levelt et al., 2006a, b), and GOME-2 (Callies et al., 2000). The global coverage available from space-borne instruments has been proven useful in estimating the large-scale distribution of NO_x sources in studies combining the satellite data with information from global scale models (Martin et al., 2003; Jaeglé et al., 2005; van der A et al., 2008; Boersma et al., 2008a). The gradually improving resolution of space-borne UV/VIS instruments (GOME pixel size: $40\times320\,km^2$, GOME-2: $40\,km\times80\,km^2$, SCIAMACHY: $30\times60\,km^2$, OMI: up to $13\times24\,km^2$ at nadir) increasingly allows them to detect NO_2 pollution features on a regional scale. Bertram et al. (2005), for example, used SCIAMACHY measurements to investigate the daily variations in regional soil NO_x emissions, and Blond et al. (2007) compared columns from a mesoscale model with SCIAMACHY columns over Western Europe. The comparatively high resolution of the OMI instrument was demonstrated valuable in analyzing urban-scale pollution and its changes in time (Wang et al., 2007; Boersma et al., 2009).

A good knowledge of the precision and accuracy of the observations is important, too. However, due to the complex retrieval procedure this is more challenging to achieve for satellite observations than for ground-based in situ measurements. A detailed general error analysis for satellite NO_2 retrievals was presented by Boersma et al. (2004). It shows that the retrieval uncertainties are dominated by the uncertainty in the estimate of the tropospheric air mass factor, which is of the order of 20–30% for polluted pixels. Key input parameters for the calculation of the tropospheric air mass factor are cloud fraction, surface albedo, and a priori NO_2 profile shape, each having its own uncertainty. Extending on this work, Boersma et al. (2007) identified a new type of error associated with the improved spatial resolution of recent sensors like OMI. True variations of surface albedo and NO_2 profile shapes at the scale of individual satellite pixels can no longer be resolved by the input data sets used in the retrievals which are traditionally obtained from coarse global climatologies and models. To illustrate this problem, Fig. 1 shows the OMI overpass over central Europe on 3 January 2006 together with the outlines of two input parameter grids used in the Dutch OMI NO_2 (DOMINO) retrieval (Boersma et al., 2008b).

Our prime motivation for this study was to obtain reliable NO_2 column estimates over Switzerland. In Switzerland as well as in most other countries in Europe, NO_2 is one of the key air pollutants and despite significant reductions since the late 1980s due to the introduction of exhaust after-treatment for stack emissions, 3-way catalysts and other measures, its concentrations are still frequently exceeding the air quality limits. This is particularly true for the heavily industrialized and densely populated Po Valley in Northern Italy which is one of the most polluted places in Europe and which affects air quality in southern Switzerland. The Swiss plateau and the Po Valley are thus our principal areas of interest. Both are located in the vicinity of the Alps (see Fig. 1) which creates additional challenges to the retrieval. Surface pressure (or elevation) is a retrieval parameter that in principle could be estimated accurately. However, to ensure consistency between a priori NO_2 profiles and surface pressure, the latter is typically obtained from the same coarse resolution data set. Schaub et al. (2007) demonstrated that this can lead to significant systematic errors over and in the surroundings of mountainous terrain. The potential errors were quantified based on a sensitivity analysis for a few selected clear sky SCIAMACHY pixels and a priori profile shapes.

In this paper we extend on the study of Schaub et al. (2007) and present a simple approach for a more accurate treatment of the surface topography which preserves consistency with the coarse resolution a priori NO_2 profiles. This is a first step towards a more accurate NO_2 retrieval tailored to Central Europe for which we intend to replace all input parameters by higher resolution data sets. The effect of inaccurate surface pressures is quantified by reprocessing extended time periods with accurate pixel-average surface pressures and comparing original and enhanced retrieval for different seasons separately. A sensitivity study is performed to investigate the dependence of the topography-related error on other forward model parameters including a priori profile shape, surface albedo, solar zenith angle (SZA) and cloud parameters.

Finally, to demonstrate the potential improvement of this approach, NO_2 columns from the original and enhanced retrieval are compared with ground-based in situ observations over the Swiss plateau (station Taenikon) and selected stations in the Po Valley in Italy where the effects of inaccurate surface pressure are the largest.

Despite our focus on the Alpine domain, the method proposed here will be applicable to any other region of the globe with complex topography and can easily be transferred to other retrieval algorithms.

2 Data and methods

2.1 OMI tropospheric NO_2 observations

The Dutch-Finnish OMI instrument onboard the Earth Observing System (EOS) Aura satellite launched in 2004 offers greatly enhanced spatial and temporal (daily global coverage) resolution as compared to its predecessors. The Aura satellite (Schoeberl et al., 2006) passes over the equator in a sun-synchronous ascending polar orbit at 13:45 local time. The NO_2 vertical columns studied in this work are basically calculated in the same way as the DOMINO (Dutch OMI NO_2) product data version 1.0.2 available from ESA's TEMIS project (Tropospheric Emission Monitoring Internet Ser-

AMTD

2, 781–824, 2009

vice, www.temis.nl). Deviations will be detailed in Sect. 2.2. Data is available since October 2004. As opposed to the Dutch near-real time product, DOMINO is a more accurate post-processing data set based on a more complete set of OMI orbits, improved Level 1B (ir)radiance data (collection 3, Dobber et al., 2008), analyzed meteorological fields rather than forecast data, and actual spacecraft data (Boersma et al., 2007). These improvements make DOMINO the recommended product for scientific use (Boersma et al., 2008b). The improved instrument calibration parameters used in collection 3 lead to much lower across-track variability, or stripes, in the OMI NO_2 products and therefore no de-striping is applied. Another important change from earlier versions is that the surface albedo is now based on the Koelemeijer et al. (2003) database. Detailed descriptions of the algorithm for the DOMINO data product are given in Boersma et al. (2007, 2008b, 2009).

The starting point in this study is the tropospheric slant columns (SCD_{trop}) obtained from the measured slant columns by subtraction of the stratospheric slant columns. In the DOMINO retrieval the stratospheric slant columns are obtained with a data-assimilation approach using the TM4 global chemistry transport model (Dentener et al., 2003). The vertical tropospheric column (VTC) is then derived by dividing SCD_{trop} by the tropospheric air mass factor (AMF_{trop}).

AMF_{trop} depends on the a priori trace gas profile x_a and a set of forward model parameters $\hat{b}$ including cloud parameters (cloud fraction, cloud pressure), surface albedo, surface pressure and viewing geometry. For small optical thickness, the altitude dependence of the measurement sensitivity to the atmospheric species of interest (calculated with a radiative transfer model) can be decoupled from the shape of the vertical trace gas profile (calculated e.g. with an atmospheric chemistry transport model). AMF_{trop} can then be written as follows (Palmer, 2001):

$$AMF_{trop} = \frac{\sum_l m_l(\hat{b}) x_{a,l}}{\sum_l x_{a,l}} \qquad (1)$$

where l is an index denoting the atmospheric layer. The altitude dependent box air mass factors m_l are calculated with a pseudo-spherical version of the DAK radiative transfer model (Stammes, 2001; de Haan et al., 1987). For computational efficiency, a lookup-table with precalculated box air mass factors at discrete points of the forward model parameters is used, and the values for a given set of parameters are obtained by linear interpolation.

The a priori NO_2 profile x_a (molecules cm^{-2}) for every location is obtained from the TM4 model. The profiles are collocated daily with a model output at overpass time of the satellite. The TM4 model version used for DOMINO has a horizontal resolution of 2° latitude by 3° longitude and 34 terrain-following hybrid layers extending from the surface to 0.38 hPa. The layers are defined by two sets of hybrid level coefficients a and b:

$$
\begin{aligned}
p_{b,l} &= a(l) + p_{\mathrm{TM4}} \cdot b(l) \\
p_{t,l} &= a(l+1) + p_{\mathrm{TM4}} \cdot b(l+1)
\end{aligned}
\qquad (2)
$$

where $p_{b,l}$ and $p_{t,l}$ are the bottom and top pressure of layer l (l=1...34), and p_{TM4} is the TM4 model surface pressure, which equals to the bottom pressure of layer one (since $a(1)=0$ and $b(1)=1$). The mid pressure of each layer is defined as the mean of $p_{b,l}$ and $p_{t,l}$. Over marked topography, p_{TM4} may strongly deviate from the effective pixel-average surface pressure (denoted p_{eff} in the following) due to the coarse resolution of the TM4 model data, which is responsible for the systematic retrieval errors discussed in this study.

In Sect. 3.3 we will show that these errors are particularly important for cloudy scenes. The AMF for a partly cloudy scene is determined with the independent pixel approach (Boersma et al., 2007), which assumes that the air mass factor can be written as a linear combination of a cloudy and a clear sky air mass factor:

$$
\mathrm{AMF}_{\mathrm{trop}} = w\,\mathrm{AMF}_{\mathrm{cloud}}(p_c) + (1-w)\,\mathrm{AMF}_{\mathrm{clear}}(p_s) \qquad (3)
$$

where $\mathrm{AMF}_{\mathrm{cloud}}$ is the AMF for a completely cloudy pixel, and $\mathrm{AMF}_{\mathrm{clear}}$ the AMF for a completely cloud-free pixel. A single cloud pressure p_c is assumed within a given viewing scene, p_s is the surface pressure. The AMF_{cloud} is obtained with Eq. (1) with m_l=0 for all layers below cloud. The cloud radiance fraction w is defined as

$$w = \frac{f_{cl} I_{cl}}{f_{cl} I_{cl} + (1 - f_{cl}) I_{cr}} \tag{4}$$

where f_{cl} is the OMI effective cloud fraction, and I_{cl} and I_{cr} are the radiances for cloudy and clear scenes, respectively. I_{cl} mainly depends on the viewing geometry and the assumed cloud albedo (Koelemeijer et al., 2001) and I_{cr} depends on surface albedo and viewing geometry. The cloud fraction and cloud-top heights are retrieved from the VIS-channel using the O_2-O_2 absorption features at 477 nm (Acarreta et al., 2004).

2.2 Retrieval with effective pixel-average surface pressures

To calculate more accurate effective pixel-average surface pressures, the topography height from the global digital elevation model GTOPO30 available on a high resolution (~1×1 km^2) was averaged over each OMI pixel. The resulting effective terrain height $h_{\rm eff}$ of each pixel was converted to an effective surface pressure $p_{\rm eff}$ based on the TM4 surface temperature $T_{\rm surf}$, surface pressure $p_{\rm TM4}$ and topography height $h_{\rm TM4}$ available in the DOMINO product. The conversion follows the hypsometric equation and the assumption that temperature changes linearly with height, which is often used for reducing measured surface pressures to sea level (Wallace and Hobbs, 1977).

$$p_{\rm eff} = p_{\rm TM4} \times \left(\frac{T_{\rm surf}}{(T_{\rm surf} + \Gamma(h_{\rm TM4} - h_{\rm eff}))} \right)^{-g/R\Gamma} \tag{5}$$

where R=287 J kg^{-1} K^{-1} is the gas constant for dry air, Γ=6.5 K km^{-1} the lapse rate, and g=9.8 m s^{-2} the acceleration by gravity.

The absolute difference between effective and TM4 terrain height $\Delta h = h_{\rm eff} - h_{\rm TM4}$ is plotted in Fig. 2, which demonstrates the large mismatch in the Alpine region. In the TM4 model, the topography is averaged over extended grid elements (cf. Fig. 1) leading to an underestimation of the effective elevation of up to 1400 m for the highest mountains near the border between Switzerland, France and Italy. Conversely, there is an overestimation in the surrounding areas of up to 500 m over the Swiss plateau and more than 700 m over the Po Valley in Italy.

With the other forward model parameters kept the same as in the DOMINO product, the AMF_{trop} and NO_2 VTC was first calculated for the TM4 surface pressure p_{TM4}, and then recalculated for the effective surface pressure p_{eff} for all the pixels within the domain of interest (latitude between 44° N and 52° N, longitude between 5° E and 12° E) from January 2006 to May 2008. The retrieval with p_{TM4} in principle reproduces the DOMINO product. However, to obtain more accurate results we found it necessary to recompute the lookup-table of box air mass factors with additional levels of the forward model parameter "surface pressure". We increased the number of surface pressure levels from 10 to 17, allowing for more accurate interpolation in the lower troposphere. Furthermore we eliminated a problem in the calculation of box air mass factors close to the surface: for any given pressure the algorithm interpolates the box AMF between the values at the two neighboring pressure levels of the lookup table, but the lower level may be located below the surface. In that case the box AMF at the lower level was assigned an unphysical value of zero, which resulted in a too low interpolated box AMF. This is an additional improvement that will be implemented in future versions of the DOMINO product. Thus, it should be kept in mind that even our product retrieved with p_{TM4} is not identical to the DOMINO data set.

For the retrieval with p_{eff} the a priori NO_2 profiles had to be rescaled vertically to be consistent with p_{eff}. This scaling is performed in a way that preserves mixing ratios rather than subcolumns:

$$x_{a,l}^{\mathrm{eff}} = x_{a,l} \times \left(\frac{p_{b,l}^{\mathrm{eff}} - p_{t,l}^{\mathrm{eff}}}{p_{b,l} - p_{t,l}}\right) \qquad (6)$$

where $x_{a,l}^{\mathrm{eff}}$ and $x_{a,l}$ are the a priori NO_2 profile with p_{eff} and p_{TM4} respectively. $p_{b,l}^{\mathrm{eff}}$ and $p_{t,l}^{\mathrm{eff}}$ are obtained following Eq. (2) with p_{eff} replacing p_{TM4} in the formula. An example for the difference between original and rescaled profile is presented in Fig. 8.

3 Results and discussion

3.1 Monthly mean and annual cycle

The relative change in retrieved NO_2 VTC defined as $(VTC_{eff}-VTC_{TM4})/VTC_{TM4}$ was calculated for all snow-free (surface albedo <0.6) clear sky OMI pixels. Corresponding monthly mean maps are plotted exemplarily for December and June 2006 in Figs. 3 and 4, respectively, and for two different thresholds for the cloud radiance fraction of 50% (a), and 10% (b). Observations over snow were eliminated because for these pixels it is known that the contrast between cloud and the surface is too low to make a proper distinction between the two, leading to an incorrect effective cloud fraction (King et al., 1992), and therefore an ill-determined cloud pressure and less reliable retrieval.

Comparing the relative change in retrieved NO_2 VTCs in Figs. 3 and 4 to Δh in Fig. 2 shows that for negative $\Delta h(h_{eff}<h_{TM4}$, e.g. over the Swiss Plateau and the Po Valley) NO_2 VTCs are underestimated when retrieved with TM4 surface pressure while for positive $\Delta h(h_{eff}>h_{TM4}$, e.g. over the Alps) the columns are overestimated by more than 20% near the highest mountain ranges. Since NO_2 is generally low over the mountain regions and the retrieval is more uncertain due to the complex topography and snow, we focus on the more polluted areas over the planes. Comparing Figs. 3 and 4 further suggests that the relative changes in NO_2 VTCs are depending on season. For example, NO_2 VTCs are underestimated by more than 25% over some places in the Po Valley in December whereas in June the differences do not exceed 15%. Another interesting finding is that there is an obvious difference in the results for the different cloud radiance fraction criteria. For areas with negative Δh, a 50% threshold results in more serious underestimation of NO_2 VTCs than a 10% threshold, and this difference is much more obvious in December than in June. The large sensitivity of the results to the selected threshold implies that the relative change in NO_2 VTCs is particularly large for the cloudy part of the pixels, especially in winter. This issue will be discussed in Sect. 3.3.

For illustration of the seasonal differences, two small areas were selected over the Swiss Plateau and the Po Valley (labels A and B in Fig. 2), respectively. The averaged Δh of the selected areas are about 400 and 700 m, respectively, corresponding to a difference of about 45 hPa and 80 hPa between p_{TM4} and p_{eff}. Figures 5 and 6 show the time series of monthly averaged NO_2 VTCs from January 2006 to May 2009 for all pixels centered in areas A and B, respectively, retrieved with p_{TM4} (black solid line with square symbols) and p_{eff} (black dashed line with diamonds). Winter months have much higher NO_2 VTCs than summer months due to the increased lifetime of NO_2 (Schaub et al., 2007) and reduced vertical mixing. At the same time, both the absolute (black solid lines with crosses) and relative changes in NO_2 VTCs (grey lines) exhibit a seasonal cycle with higher values in winter months. However, the seasonal cycle of the changes does not necessarily align with the seasonal cycle of NO_2 VTCs itself. For pixels with a cloud radiance fraction lower than 50% the underestimation of NO_2 VTCs reaches values larger than 20% in both areas in some winter months (Figs. 5a, 6a). The changes in NO_2 VTCs are generally smaller over the Swiss Plateau than over the Po Valley consistent with the smaller altitude shift. In summer, the relative change is typically of the order of 5% and the absolute change is rather small due to the much lower NO_2 VTCs. With a cloud radiance fraction threshold of 10%, the changes in NO_2 VTCs have a much less pronounced seasonal cycle for both areas (Figs. 5b, 6b). The cause of this difference will be discussed in Sect. 3.3.

3.2 Sensitivity analysis for cloud free pixels

According to Eq. (1) the AMF_{trop} is entirely determined by the profile of the altitude dependent box air mass factors m_l and by the a priori NO_2 profile shape obtained from the TM4 model. The effect of a surface pressure change on these profiles is illustrated in Figs. 7 and 8 for the two selected pixels separately. Comparing Fig. 7a and b it can be seen that the profiles of m_l differ significantly between the two pixels due to the large difference in the forward parameters. In the upper atmosphere the values approach the geometric air mass factor which is determined by the SZA and

AMTD
2, 781–824, 2009

viewing zenith angle (VZA) (Palmer, 2001). The trends of the two profiles are similar with decreasing m_l towards the ground, which represents the decreasing sensitivity of the satellite instrument towards the surface due to increased scattering of light above the level of interest.

For a systematic analysis of the influence of the different retrieval parameters on the topography-related NO_2 error, two sets of forward parameters and a priori NO_2 profiles corresponding to the two pixels on 4 August and 1 December 2006 were selected to represent typical summer and winter conditions over the Po valley, respectively. The individual effects of the a priori NO_2 profile, SZA, and albedo as well as their combined effects were then investigated by systematically replacing each parameter by its value of the opposing season. The corresponding retrieval parameter settings are listed in Table 1, and the results are shown in Fig. 9. The TM4 surface pressure was assumed to be 928 hPa in all cases as a reference point and the effective surface pressure p_{eff} was varied about this point within reasonable limits thereby shifting up or down the profiles of box air mass factors and a priori profiles as described in Sect. 2.2. In the Po Valley, the differences between p_{eff} and p_{TM4} are of the order of 80 hPa. The relative changes in $\mathrm{AMF_{trop}}$ and NO_2 VTCs for this specific point on the sensitivity lines in Fig. 9 are summarized in Table 1.

The shape of the a priori NO_2 profile is an important factor in determining the $\mathrm{AMF_{trop}}$ (see Eq. 1). Due to the poor spatial resolution of the TM4 model the a priori NO_2 profile varies only slowly in space such that our selected profile is representative for large parts of the Po Valley. As seen in Fig. 8, the selected winter profile exhibits a pronounced peak in the boundary layer since vertical mixing is generally weak in winter, and both the lifetime of NO_x and the emissions are enhanced in this season (Richter et al., 2002; Jaeglé et al., 2005). In contrast, the selected summer profile shows a much lower NO_2 abundance near the ground resulting from enhanced vertical mixing and a reduced lifetime. Figure 9a shows how the sensitivities of the $\mathrm{AMF_{trop}}$ and NO_2 VTCs to varying surface pressure change when replacing the winter profile by the summer profile while keeping all other parameters constant. In comparison to summer,

AMTD
2, 781–824, 2009

Improved tropospheric NO_2 retrieval for satellite observations

Y. Zhou et al.

the more pronounced a priori NO_2 profile in winter results in a stronger sensitivity of the retrieved NO_2 VTCs to errors in the assumed surface pressure in agreement with the findings of Schaub et al. (2007). This is understandable since changes in surface pressure most strongly affect the box air mass factors m_l at the lowest levels, and this effect is amplified in the computation of AMF_{trop} if the a priori profile predicts most of the NO_2 at these levels.

The solar zenith angle is another parameter changing strongly with season. For the selected location in the Po valley the SZA varies from 31° on 4 August to 70° on 1 December. Results for these two SZA are presented in Fig. 9b. For the larger SZA in winter, the relative changes in AMF_{trop} and NO_2 VTCs are more sensitive to differences between p_{TM4} and p_{eff} than for the smaller angles in summer. This effect thus adds to the differences observed between winter and summer.

Finally, the albedo is another parameter potentially changing with season. For the selected location the albedo varies quite strongly from 0.057 on 4 August to 0.116 on 1 December. In Fig. 9c, surprisingly and in contrast to the two previous parameters, even though the largely different albedos in winter and summer seem to have a significant effect on the absolute values of AMF_{trop}, they have a negligible influence on the sensitivity of relative changes in AMF_{trop} and NO_2 VTCs to changing surface pressure, given the retrieval parameter settings in Table 1.

Figure 9d illustrates the combined effect of the three parameters above. For the selected location in the Po valley, where p_{TM4} is 928 hPa and p_{eff} is 1008 hPa, the relative NO_2 VTCs change for cloud-free pixels is about 8% in winter and 4% in summer. The sensitivity of the retrieval error to the surface pressure error is thus almost twice as large in winter as in summer which is mainly a consequence of the differences in a priori profile shape and SZA as described above. The other forward model parameters VZA and relative azimuth angle (AZA) were not included in this sensitivity study as they do not vary with season but rather within a single swath.

AMTD
2, 781–824, 2009

3.3 Sensitivity analysis for cloudy pixels

To illustrate the effect of the inaccurate topography for partly cloudy pixels, we took the same forward model parameters as for the cloud-free pixel presented in Fig. 7b but assumed a cloud fraction of 15% and a cloud top pressure of 900 hPa. The profile of box AMFs of the completely cloudy part is shown in Fig. 10a, and the corresponding profile of the partly cloudy pixel in Fig. 10b, which is the weighted sum of the values in Fig. 7b and Fig. 10a. Clouds are modeled as opaque Lambertian reflectors with an albedo of 0.8 (Acarreta et al., 2004). The sensitivity is enhanced above the bright cloud but drops to zero below the top of the opaque cloud as seen in Fig. 10a. The box AMF corresponding to the pressure just larger than the cloud top pressure (903 hPa) behaves like a transition point, since the cloud is located within this layer, and the fraction of the layer above the cloud still has non-zero m_l. This sudden change in m_l is also reflected in the profile of effective box AMFs of the partly cloudy pixel shown in Fig. 10b. Below cloud top the box AMFs drop to values much smaller than for the cloud free case in Fig. 7b.

AMF_{trop} is determined by the m_l of the partly cloudy pixel and the a priori NO_2 profile according to Eq. (1). Figures 3 and 4 suggest that the AMF_{trop} is generally more sensitive to the change in terrain height for cloudy pixels than for cloud free pixels. The reason for this is illustrated in Fig. 11 showing the situation for a partly cloudy pixel and a low level cloud. Shifting the surface to a lower effective pixel altitude (right hand part of Fig. 11), e.g. over the Po Valley, results in more levels becoming poorly visible to the satellite (as expressed by the rapid drop of m_l below cloud top) and effectively places a larger fraction of the polluted part of the NO_2 profile below the cloud (red line in Fig. 11b). This results in a much lower AMF_{trop} and correspondingly higher NO_2 VTC.

The sensitivity to the surface pressure change depends on cloud top pressure and the a priori NO_2 profile shape. To demonstrate this the relative changes in AMF_{trop} and NO_2 VTC are shown in Fig. 12 as a function of the change in surface pressure for two different cloud pressures for the winter pixel (retrieval parameters as in case A1 in Table 1). The NO_2 VTC retrieved with p_{eff}=1008 hPa instead of p_{TM4}=928 hPa is close to 40% higher when the cloud is located close to the surface (cloud pressure=900 hPa), which is a much larger change than for the cloud free situation. However, when the cloud is higher at 850 hPa the increase is only about 10%. Interestingly, the very high sensitivity to surface pressure only occurs over a range of about 50 hPa below cloud top, which corresponds to the depth of the boundary layer with elevated NO_2 in Fig. 8b. Thus, for a cloud top located inside the polluted boundary layer the retrieval error due to inaccurate surface pressure is large, especially in the winter season with pronounced NO_2 in the boundary layer. Conversely, when the cloud top is located above the boundary layer, the retrieval error is comparatively small and similar to the cloud free case. Low clouds were frequently observed over some areas in the Po Valley during winter. For example, the monthly mean cloud pressure over area B in Fig. 2 was 917 hPa in December 2006, which contrasts with a much lower pressure of 789 hPa in June 2006. The predominance of low clouds likely explains the very high relative changes in retrieved NO_2 VTCs in December 2006 over some areas in Fig. 3a.

4 Validation

4.1 Calculation of tropospheric NO_2 VTCs from ground-based measurements

In-situ ground-based measurements of NO_2 for the period January 2006 to December 2007 were obtained from two sources, from the Swiss National Air Pollution Monitoring Network (NABEL) (http://www.bafu.admin.ch/luft/00612/00625/index.html) for stations over the Swiss plateau, and from the Lombardy Regional Agency for Environmental Protection (ARPA), Italy, for stations in the Po Valley/Milano area (http://www.ambiente.regione.lombardia.it). From a total of more than 100 stations only 35 were selected for the validation. All the selected stations are background stations not affected by local traffic or industrial pollution sources, and have a data coverage of more than 80% at the time of the OMI overpass during the analysis period. At these stations, nitrogen oxides are measured using commercial instruments with molybdenum converters. NO_2 is catalytically converted to NO on a heated molybdenum surface, and then measured as NO by chemiluminescence after reaction with ozone. It is well known that these converters are sensitive not only to NO_2 but also to other odd nitrogen species such as PAN, HNO_3 and organic nitrates (Winer et al., 1974; Grosjean and Harrison, 1985; Steinbacher et al., 2007). Nevertheless, it is the standard method applied in air quality monitoring networks. In a similar study using the Lombardy station network for validation of GOME observations, Ordóñez et al. (2006) quantified the interference in the molybdenum converter at GOME overpass time following the approach of Schaub et al. (2006), based on simultaneous measurements of surface NO_2 performed with a photolytic converter (selective for NO_2 only) and a molybdenum converter at the rural site Taenikon (47.47° N, 8.90° E, 539 m above sea level), Switzerland, during the period 1995–2001. The ratios of the monthly medians of these two measurements on sunny days (photolytic divided by molybdenum) at GOME overpass time (~10:30 local time) were then used as factors to correct the molybdenum converter measurements. As a first approximation, we followed the same approach yet quantifying the interference at the overpass time of OMI instead of GOME. The calculated monthly correction factors are shown in Table 2. The ratios show a clear seasonal cycle with a summertime minimum. This is expected since during the warm season the photochemistry leads to a higher production of oxidized nitrogen species such as HNO_3 and PAN which results in a more pronounced overestimation of the NO_2 surface concentrations by the molybdenum measurements. The ratios at OMI overpass time differ by less than 5% from those of Ordóñez et al. (2006) at GOME overpass time from October to January but are about 10% lower in the other months due to the more pronounced diurnal cycles of the interference with a larger overestimation of NO_2 concentrations in the afternoon than in the morning (Steinbacher et al., 2007).

Monthly mean ratios can not reflect the potentially large temporal and spatial variations in the ratios due to varying photochemistry. In this study we therefore adopt the refined correction method proposed by Steinbacher et al. (2007) which models the ratios by a multiple linear regression approach using daily O_3 mixing ratios as a proxy for photochemical activity and month as a factor variable to estimate the seasonal variation. We used the same regression coefficients as Steinbacher et al. (2007) which are based on an analysis of the same Taenikon data used by Ordoñez et al. (2006). We then corrected the NO_2 measurements for each station separately using the ozone data of the respective station if available. For 7 out of 35 stations no ozone measurements were available and therefore the monthly median ratios based on Taenikon measurements in Table 2 had to be used. For comparison, Table 2 also lists the monthly median correction factors deduced from the regression approach for the 28 stations with O_3 measurements. The regression based median ratios are slightly smaller (up to −6.3%) in winter, but are significantly higher in the other seasons compared to Taenikon monthly median ratios with a maximal relative difference as high as 58.4% in August. The reason for this is that the Po valley stations tend to be more polluted and closer to the pollution sources than the station Taenikon and therefore the interferences from higher oxidized NO_y species tend to be smaller.

Hourly NO_2 measurements averaged over 13:00–14:00 local time were used for the comparison with the NO_2 VTCs measured from OMI at about 13:30 LT. Only measurements coincident with a valid OMI observation (see selection criteria below) and only days with a surface NO_2 mixing ratio larger than 1 ppb were considered since the instrument detection limit for NO_2 is approximately 1 ppb (NABEL, 2007). For quantitative comparison with the satellite observations, corrected NO_2 mixing ratios measured at the surface were scaled to NO_2 VTCs using the same TM4 vertical NO_2 profiles used also as a priori. These profiles are representative for the time and location of each OMI observation. The "ground based in-situ NO_2 VTCs" were calculated according to:

$$\mathrm{VTC}_G = \frac{\mathrm{VTC}_{\mathrm{TM4}}}{S_{\mathrm{TM4}}} \times S_G \tag{7}$$

where S represents the surface level mixing ratio and subscript G denotes ground based measurement. $\mathrm{VTC}_{\mathrm{TM4}}$ is calculated by summing up the TM4 model subcolumns from the surface to the tropopause level. S_{TM4} is the NO_2 mixing ratio of the model at the lowest level. For comparison with the OMI NO_2 VTCs retrieved with p_{TM4}, the original TM4 profile was used. For comparison with the OMI NO_2 VTCs retrieved with p_{eff}, however, the profile scaled to the effective surface pressure following Eq. (6) was used.

The selection of OMI pixels was based on the following criteria: (1) pixel center within 10 km of the station and east-west extension of the pixel of less than 70 km, (2) cloud radiance fraction lower than 50%, (3) albedo smaller than 0.6 to exclude snow cover. If there was more than one pixel meeting the criteria on the same day then the OMI pixel with the smallest effective cloud fraction was selected. The thresholds for these criteria were set to balance data quality with a sufficient number of measurements for good statistics.

4.2 Comparison of in situ and OMI tropospheric NO_2 VTCs

Figure 13 shows the correlation coefficients (r^2) between in-situ and OMI NO_2 VTCs retrieved with p_{eff}. For most of the stations, the in-situ NO_2 VTCs are well correlated with the satellite observations, with r^2 ranging from 0.3 to 0.7 for, on average, 180 data points per station. Poorer correlations are observed for a few elevated stations in the pre-Alps. Due to enhanced spatial variability, both the representativeness of the surface measurement and our approach of surface measurement correction become more uncertain for these stations.

The measurement sites are classified by land use type as rural, suburban and urban. The medians of the ratios at each station between monthly means of the OMI and in-situ NO_2 VTCs are shown in Fig. 14 for each station type separately. For urban stations, the ratios are closer to unity in all four seasons compared to rural and suburban stations. In Boersma et al. (2009), good agreement between OMI and in situ measurements was also found for Israeli urban stations. The retrieval with accurate surface pressure p_{eff} improves the agreement in winter for both urban and suburban stations where the retrieval with p_{TM4} underestimates NO_2 VTCs. For rural and suburban stations, the ratios exhibit a pronounced seasonal variation with highest ratios in spring months suggesting a significant overestimation of the OMI NO_2 VTCs in this season. It is important to note, however, that in these cases the absolute values and also the absolute differences between OMI and in-situ NO_2 VTCs are small, with an average absolute overestimation of 4.3 and 3.4 (10^{15} molecules cm^{-2}) for rural and suburban stations respectively. Lamsal et al. (2008) reported similar differences between OMI and in situ measurements over North American with strongest overestimation in summer. They concluded that the larger seasonal bias at rural sites suggests an incomplete removal of stratospheric NO_2 which has a larger relative effect where tropospheric NO_2 columns are lower. However, different from Lamsal et al. (2008), the ratios are higher than one in most of the seasons for rural and suburban stations in our study, which may be explained by the use of different OMI NO_2 products (standard product from NASA versus our modified DOMINO product). As suggested by Bucsela et al. (2008), the NASA and KNMI algorithms produce significantly different tropospheric NO_2 amounts mainly due to the different retrieval parameters used.

Two examples of the comparison between OMI and in-situ NO_2 VTCs at individual stations are shown in Fig. 15 for the rural station Motta (45.29° N, 9° E) and the urban station Pavia (45.19° N, 9.16° E). The OMI VTCs follow the seasonal variation of the in situ VTC data very well, but the OMI columns tend to be too high at the rural station Motta in all months, and to be too low at the urban station Pavia in winter and fall. A weighted least squares orthogonal regression was performed for each station which considers the uncertainties in both measurements and minimizes the distances in both y- and x-direction by a chi-square minimization procedure (Press et al., 1992). The uncertainties of the OMI NO_2 VTCs were taken to be the estimates of the tropospheric column error as provided in the DOMINO product following the approach of Boersma et al. (2004). For the majority of the OMI pixels, this uncertainty ranges from 30% to 60% of the NO_2 VTCs. The uncertainties of the in-situ NO_2 VTCs were computed as the square root of the sum of the squares of two independent errors: (1) The representativeness uncertainty, which depends on how well the TM4 NO_2 vertical profile used in calculating the in-situ NO_2 column represents the real NO_2 profile at the location of the station, and also how well the station NO_2 represents the NO_2 abundance over the whole extent of an OMI pixel. This uncertainty is assumed to be 20% of the in-situ NO_2 VTCs. (2) The uncertainty due to the in situ measurement error, which is estimated as the sum of the instrument detection limit (1 ppb) and a measurement accuracy of 10% of the NO_2 mixing ratio (NABEL, 2007). The uncertainty of the in situ NO_2 is converted to a column uncertainty using Eq. (7). For both stations the slope of the regression line is closer to one when retrieved with p_{eff} implying a better agreement between in situ and OMI VTCs. For the station Pavia this is clearly a result of the better agreement of OMI NO_2 columns retrieved with p_{eff} in winter and fall. It is interesting to see that both the slope and r^2 for the rural station Motta are improved with p_{eff} while the corresponding monthly mean OMI VTCs tend to be more strongly overestimated. In summary, it may be concluded that the amplitude of the seasonal variations of NO_2 VTCs over the Po Valley and the Swiss Plateau is better captured with our enhanced retrieval due to the increases in autumn and winter while the problem of overestimation of the lowest columns in spring and summer remains.

5 Conclusions

An improved NO_2 retrieval for satellite observations over mountainous terrain was presented and applied to more than two years of OMI observations over the Alpine region and the adjacent planes. The method eliminates topography-related biases caused by the use of too coarse surface pressure (or altitude) data in operational retrievals. Accurate pixel-average surface pressures were calculated by correcting the original values with information from a high resolution topography model. A priori NO_2 profiles used in the retrieval were then scaled to the new surface pressures and tropospheric AMFs and NO_2 VTCs were recomputed using a modified version of the DOMINO retrieval algorithm.

The comparison between original and enhanced retrieval indicates that the original coarse surface pressure data set lead to a significant overestimation of NO_2 VTCs over the Alps and an underestimation over the adjacent planes. For clear sky observations with a threshold for the cloud radiance fraction of 50% the original retrieval is about 25% too low in winter and about 5% in summer over the Po Valley and the Swiss Plateau. However, these errors are much smaller when a more stringent threshold for the cloud radiance fracton of 10% is applied, which reduces the data set to essentially cloud-free pixels.

In a previous study we reported on larger topography-related errors of the order of 13–38% for cloud free pixels over the Swiss plateau (Schaub et al., 2007). However, these results were based on a few selected cases only and were affected by a problem in the retrieval algorithm (see Sect. 2.2) which resulted in too low box air mass factors close to the ground and therefore a too large sensitivity to surface pressure changes.

The strong dependence of our results on the chosen cloud radiance threshold suggests that the AMFs calculated for the cloudy part of the pixels are more sensitive to errors in surface pressure than the AMFs of the clear part. This was confirmed by a detailed analysis for a partly cloudy pixel which further revealed that this sensitivity is particularly large when the cloud top is located inside the polluted boundary layer.

To examine the reason for the pronounced seasonal differences of our results we performed a systematic sensitivity analysis of the dependence of the topography-related error on those retrieval parameters potentially changing with season. For cloud free pixels, the seasonal differences in the a priori NO_2 profile shape was found to be the dominating factor explaining a major fraction of the different sensitivities to the surface pressure error between winter and summer. Differences in SZA were also found to be important while changes in albedo had no significant effect. Overall, the sensitivity of the retrieval error to the surface pressure error is almost twice as large in winter as in summer.

To analyze the influence of the improved treatment of the topography on the quality of the retrieved NO_2 VTCs we compared the original and enhanced OMI data with NO_2

AMTD

2, 781–824, 2009

Improved tropospheric NO_2 retrieval for satellite observations

Y. Zhou et al.

VTCs deduced from ground-based in situ measurements. Our validation focused on 35 selected stations over the Swiss plateau (station Taenikon) and the Po Valley in Italy where the effects of inaccurate surface pressure are the largest. Only background stations in urban, suburban and rural environments were selected as they are less affected by nearby sources and are therefore expected to be representative for their respective environment. The in-situ NO_2 measurements were corrected for known interferences from higher oxidized nitrogen species such as PAN and HNO_3 using ozone as a proxy for photochemical activity as proposed by Steinbacher et al. (2006). Corrected NO_2 mixing ratios were then scaled to NO_2 VTCs using NO_2 vertical profiles from the TM4 model. With the accurate surface pressure data set, in-situ and OMI NO_2 VTCs exhibit a significant correlation (r^2=0.3–0.7) for most stations. A particularly good agreement between OMI and in situ measurements in terms of both correlation and absolute values was found for urban background stations in the Po valley. Our new retrieval further improves the agreement for both urban and suburban stations by partially correcting the underestimation of NO_2 VTCs retrieved with p_{TM4}, which is serious in winter. Since in winter and fall there exist lowest uncertainties in the correction factors applied to the in situ measurements, we are most confident with this improvement. However, for rural and suburban stations, the ratios between OMI and in-situ NO_2 VTCs exhibit an obvious seasonal variation with highest values close to 2 in spring months. Taking the uncertainties of each data point of both measurements into consideration in the regression analysis, our retrieval also shows the potential to improve the overall agreement for rural stations.

AMTD

2, 781–824, 2009

Improved tropospheric NO_2 retrieval for satellite observations

Y. Zhou et al.

Acknowledgements. This work was supported by the Swiss Federal Office for the Environment (FOEN). We thank Piet Stammes and Johan de Haan for developing the DAK radiative transfer model and allowing us to utilize it for AMF calculations. Many thanks to the OMI team at KNMI for developing the NO_2 retrieval within the DOMINO project and for making available the data through the ESA project TEMIS. We acknowledge Christoph Hüglin, Empa, for providing NO_2 and ozone measurements from the Swiss National Air Pollution Monitoring Network (NABEL) and Enrica Zenoni for corresponding data from the Regional Agency for Environmental Protection (ARPA) of Lombardy, Italy. The authors would like to thank Carlos Ordóñez and Martin Steinbacher for useful discussions and for their assistance in the validation study.

References

Acarreta, J. R., De Haan, J. F., and Stammes, P.: Cloud pressure retrieval using the O_2–O_2absorption band at 477 nm, J. Geophys. Res., 109, D05204, doi:10.1029/2003JD003915, 2004.

Bertram, T. H., Heckel, A., Richter, A., Burrows, J. P., and Cohen, R. C.: Satellite measurements of daily variations in soil NO_x emissions, Geophys. Res. Lett., 32(24), L24812 doi:10.1029/2005GL024640, 2005.

Blond, N., Boersma, K. F., Eskes, H. J., van der A, R. J., Van Roozendael, M., De Smedt, I., Bergametti, G., and Vautard, R.: Intercomparison of SCIAMACHY nitrogen dioxide observations, in-situ measurements and air quality modeling results over Western Europe, J. Geophys. Res., 112, D10311, doi:10.1029/2006JD007277, 2007.

Boersma, K. F., Eskes, H. J., and Brinksma, E. J.: Error analysis for tropospheric NO_2 retrieval from space, J. Geophys. Res., 109, D04311, doi:10.1029/2003JD003962, 2004.

Boersma, K. F., Eskes, H. J., Veefkind, J. P., Brinksma, E. J., van der A, R. J., Sneep, M., van den Oord, G. H. J., Levelt, P. F., Stammes, P., Gleason, J. F., and Bucsela, E. J.: Near-real time retrieval of tropospheric NO_2 from OMI, Atmos. Chem. Phys., 7, 2103–2118, 2007, http://www.atmos-chem-phys.net/7/2103/2007/.

Boersma, K. F., Jacob, D. J., Bucsela, E. J., Perring, A. E., Dirksen, R., van der A, R.J., Yantosca, R.M., Park, R.J., Wenig, M., Bertram, T. H., and Cohen, R. C.: Validation of OMI tropospheric NO_2 observations during INTEX-B and application to constrain NO_x emissions over the eastern United States and Mexico, Atmos. Environ., 42, 4480–4497, 2008a.

Boersma, K. F., Dirksen, R., Veefkind, J. P., Eskes, H. J., and van der A, R. J.: Dutch OMI NO_2 (DOMINO) data product HE5 data file user manual, TEMIS website, http://www.temis.nl/airpollution/no2.html, 2008b.

Boersma, K. F., Jacob, D. J., Trainic, M., Rudich, Y., DeSmedt, I., Dirksen, R., and Eskes, H. J.: Validation of urban NO_2 concentrations and their diurnal and seasonal variations observed from space (SCIAMACHY and OMI sensors) using in situ measurements in Israeli cities, Atmos. Chem. Phys. Discuss., 9, 4301–4333, 2009, http://www.atmos-chem-phys-discuss.net/9/4301/2009/.

Bovensmann, H., Burrows, J. P., Buchwitz, M., Frerick, J., Noël, S., and Rozanov, V.V.: SCIAMACHY: Mission objectives and measurement modes, J. Atmos. Sci., 56, 2, 127–150, 1999.

Bucsela, E. J., Celarier, E. A., Wenig, M. O., Gleason, J. F., Veefkind, J. P., Boersma, K. F., and Brinksma, E. J.: Algorithm for NO_2 vertical column retrieval from the Ozone Monitoring Instrument, IEEE Trans. Geosci. Rem. Sens., 44, 1245–1258, doi:10.1109/TGRS.2005.863715, 2006.

Bucsela, E. J., Perring, A. E., Cohen, R. C., et al.: Comparison of tropospheric NO_2 in situ aircraft measurements with near-real-time and standard product data from the Ozone Monitoring Instrument, J. Geophys. Res., 113, D16S31, doi:10.1029/2007JD008838, 2008.

Burrows, J. P., Weber, M., Buchwitz, M., Rozanov, V., Ladstätter-Weissenmayer, A., Richter, A., DeBeek, R., Hoogen, R., Bramstedt, K., Eichmann, K. U., Eisinger, M., and Perner, D.: The global ozone monitoring experiment (GOME): Mission concept and first scientific results, J. Atmos. Sci., 56, 151–175, 1999.

Callies, J., Corpaccioli, E., Eisinger, M., Hahne, A., and Lefebvre, A.: GOME-2: Metop's second generation sensor for operational ozone monitoring, ESA Bull., 102, 28–36, 2000.

De Haan, J. F., Bosma, P. B., and Hovenier, J. W.: The adding method for multiple scattering computations of polarized light, Astron. Astrophys, 183, 371–391, 1987.

Dentener, F., van Weele, M., Krol, M., Houweling, S., and van Velthoven, P.: Trends and interannual variability of methane emissions derived from 1979–1993 global CTM simulations, Atmos. Chem. Phys., 3, 73–88, 2003, http://www.atmos-chem-phys.net/3/73/2003/.

Dobber, M., Kleipool, Q., Dirksen, R., Levelt, P., Jaross, G., Taylor, S., Kelly, T., Flynn, L., Leppelmeier, G., and Rozemeijer, N.: Validation of Ozone Monitoring Instrument level-1b data products, J. Geophys. Res., 113, D15S06, doi:10.1029/2007JD008665, 2008.

Finlayson-Pitts, B. J. and Pitts, J. N.: Chemistry of the upper and lower Atmosphere – Theory,

Experiments and Applications, Academic Press, San Diego, CA, 2000.
Grosjean, D. and Harrison, J.: Response of chemiluminescence NO_x analyzers and ultraviolet ozone analyzers to organic air pollutants, Environ. Sci. Technol., 19, 862–865, 1985.
Jaeglé, L., Steinberger, L., Martin, R. V., and Chance, K.: Global partitioning of NO_x sources using satellite observations: Relative roles of fossil fuel combustion, biomass burning and soil emissions, Faraday Discuss., 130, 407–423, 2005.
King, M. D., Kaufman, Y. J., Menzel, W. P., and Tanré, D.: Remote sensing of cloud, aerosol and water vapor properties from the Moderate Resolution Imaging Spectrometer (MODIS), IEEE Trans. Geosci. Remote Sens., 30, 2–27, 1992.
Koelemeijer, R. B. A., Stammes, P., Hovenier, J. W., and de Haan, J. F.: A fast method for retrieval of cloud parameters using oxygen A-band measurements from Global Ozone Monitoring Experiment, J. Geophys. Res., 106, 3475–3490, 2001.
Koelemeijer, R. B. A., de Haan, J. F., and Stammes, P.: A database of spectral surface reflectivity in the range 335–772 nm derived from 5.5 years of GOME observations, J. Geophys. Res., 108, 4070, doi:10.1029/2002JD002429, 2003.
Lamsal, L. N., Martin, R. V., van Donkelaar, A., et al.: Ground-level nitrogen dioxide concentrations inferred from the satellite-borne Ozone Monitoring Instrument, J. Geophys. Res., 113, D16308, doi:10.1029/2007JD009235, 2008.
Levelt, P. F., van den Oord, G. H. J., Dobber, M. R., Mälkki, A., Visser, H., de Vries, J., Stammes, P., Lundell, J. O. V., and Saari, H.: The Ozone Monitoring Instrument, IEEE Trans. Geosci. Rem. Sens., 44, 1093–1101, doi:10.1109/TGRS.2006.872333, 2006a.
Levelt, P. F., Hilsenrath, E., Leppelmeier, G. W., van den Oord, G. H. J., Bhartia, P. K., Tamminen, J., de Haan, J. F., and Veefkind, J. P.: Science Objectives of the Ozone Monitoring Instrument, IEEE Trans. Geosci. Rem. Sens., 44, 1199–1208, doi:10.1109/TGRS.2006.872336, 2006b.
Martin, R. V., Jacob, D. J., Chance, K. V., Kurosu, T. P., Palmer, P. I., and Evans, M. J.: Global inventory of Nitrogen Dioxide Emissions Constrained by Space-based Observations of NO_2 Columns, J. Geophys. Res., 108, 4537, doi:10.1029/2003/JD003453, 2003.
Martin, R. V., Parrish, D. D., Ryerson, T. B., et al.: Evaluation of GOME satellite measurements of tropospheric NO_2 and HCHO using regional data from aircraft campaigns in the southeastern United States, J. Geophys. Res., 109, D24307, doi:10.1029/2004JD004869, 2004.
Martin, R. V., Sioris, C. E., Chance, K., et al.: Evaluation of space-based constraints on global

nitrogen oxide emissions with regional aircraft measurements over and downwind of eastern North America, J. Geophys. Res., 111, D15308, doi:10.1029/2005JD006680, 2006.

NABEL: Technischer Bericht zum Nationalen Beobachtungsnetz für Luftfremdstoffe, Empa, Dübendorf, Switzerland, 2007.

Nolin, A., Armstrong, R., and Maslanik, J.: Near-real time SSM/I EASE grid daily global ice concentration and snow extent, Digital Media, National Snow and Ice Data Center, Boulder, CO, USA, 2005.

Ordóñez, C., Richter, A., Steinbacher, M., Zellweger, C., Nüß, H., J., Burrows, P., and Prévôt, A. S. H.: Comparison of 7 years of satellite-borne and ground-based tropospheric NO_2 measurements around Milan, Italy, J. Geophys. Res., 111, D05310, doi:10.1029/2005JD006305, 2006.

Palmer, P. I., Jacob, D. J., Chance, K., Martin, R. V., Spurr, R. J. D., Kurosu, T. P., Bey, I., Yantosca, R., Fiore, A., and Li, Q.: Air mass factor formulation for spectroscopic measurements from satellites: Application to formaldehyde retrievals from the Global Ozone Monitoring Experiment, J. Geophys. Res., 106, 14539–14550, 2001.

Platt, U.: Differential Optical Absorption Spectroscopy (DOAS), in: Air monitoring by Spectroscopic Techniques, edited by: Sigrist, M. W., Chemical Analysis, 127, 27–76, 1994.

Press, W. H., Flannery, B. P., Teukolsky. S. A., and Vetterling, W. T.: Numerical recipes: The art of Scientific Computing, Cambridge Univ. Press, New York, 1992.

Richter, A. and Burrows, J. P.: Tropospheric NO_2 from GOME measurements, Adv. Space Res., 29, 1673–1683, 2002.

Schaub, D., Boersma, K. F., Kaiser, J. W., Weiss, A. K., Folini, D., Eskes, H. J., and Buchmann, B.: Comparison of GOME tropospheric NO_2 columns with NO_2 profiles deduced from ground-based in situ measurements, Atmos. Chem. Phys., 6, 3211–3229, 2006, http://www.atmos-chem-phys.net/6/3211/2006/.

Schaub, D., Brunner, D., Boersma, K. F., Keller, J., Folini, D., Buchmann, B., Berresheim, H., and Staehelin, J.: SCIAMACHY tropospheric NO_2 over Switzerland: estimates of NO_x lifetimes and impact of the complex Alpine topography on the retrieval, Atmos. Chem. Phys., 7, 5971–5987, 2007, http://www.atmos-chem-phys.net/7/5971/2007/.

Schoeberl, M. R., Douglass, A. R., Hilsenrath, E., et al.: Overview of the EOS aura mission, IEEE Trans. Geosci. Remote Sens., 44, 1066–1074, 2006.

Seinfeld, J. H. and Pandis, S. N.: Atmospheric chemistry and physics – from air pollution to climate change, John Wiley & Sons, New York, 1998.

Stammes, P.: Spectral radiance modeling in the UV-Visible range, IRS2000: in: Current problems in atmospheric radiation, edited by: Smith, W. L. and Timofeyev, Y. J., A. Deepak, Hampton, Va, USA, 385–388, 2001.

Steinbacher, M., Zellweger, C., Schwarzenbach, B., Bugmann, S., Buchmann, B., Ordóñez, C., Prevot, A. S. H., and Hueglin, C.: Nitrogen oxides measurements at rural sites in Switzerland: Bias of conventional measurement techniques, J. Geophys. Res., D11307, doi:10.1029/2006JD007971, 2007.

Vandaele, A. C., Fayt, C., Hendrick, F., et al.: An intercomparison campaign of ground-based UV-visible measurements of NO_2, BrO, and OClO slant columns: Methods of analysis and results for NO_2, J. Geophys. Res., 110, D08305, doi:10.1029/2004JD005423, 2005.

van der A, R. J., Peters, D. H. M. U., Eskes, H., Boersma, K. F., van Roozendael, M., de Smedt, I., and Kelder, H. M.: Detection of the trend and seasonal variation in tropospheric NO_2 over China, J. Geophys. Res., 111, D12317, doi:10.1029/2005JD006594, 2006.

van der A, R. J., Eskes, H. J., Boersma, K. F., van Noije, T. P. C., van Roozendael, M., de Smedt, I., Peters, D. H. M. U., and Meijer, E. W.: Trends, seasonal variability and dominant NO_x source derived from a ten year record of NO_2 measured from space, J. Geophys. Res., 113, D04302, doi:10.1029/2007JD009021, 2008.

Wallace, J. M. and Hobbs, P. V.: Atmosphere science, an introductory survey, Academic Press, California, USA, 1977.

Wang, Y. X., McElroy, M. B., Boersma, K. F., Eske, H. J., and Veefkind, J. P.: Traffic Restrictions Associated with the Sino-African Summit: Reductions of NO_x Detected from Space, Geophys. Res. Lett., 34, L08814, doi:10.1029/2007GL029326, 2007.

Winer, A. M., Peters, J. W., Smith, J. P., and Pitts Jr., J. N.: Response of commercial chemiluminescent NO-NO_2 analyzers to other nitrogen containing compounds, Environ. Sci. Technol., 8, 1118–1121, 1974.

Table 1. Retrieval parameter settings in the case studies of retrieval parameter effects on sensitivity of relative changes in AMF_{trop} (ΔAMF_{trop}) and NO_2 VTC (ΔNO_2 VTC) respect to change in surface pressure, and the results of selected surface pressure (reference point p_{TM4}=928 hPa, p_{eff}=1008 hPa).

Case	Parameter varied	a priori profile	Albedo	SZA	VZA	AZA	ΔAMF_{trop}	ΔNO_2 VTC
A1	a priori profile	winter profile	0.116	70°	11.5°	122.8°	−8.2%	8.0%
A2		summer profile	0.116	70°	11.5°	122.8°	−5.6%	5.3%
B1	SZA	summer profile	0.116	70°	11.5°	122.8°	−5.6%	5.3%
B2		summer profile	0.116	31°	11.5°	122.8°	−4.1%	4.3%
C1	albedo	summer profile	0.116	31°	11.5°	122.8°	−4.1%	4.3%
C2		summer profile	0.057	31°	11.5°	122.8°	−4.2%	4.4%
C3	combined	winter profile	0.116	70°	11.5°	122.8°	−8.2%	8.0%
C4		summer profile	0.057	31°	11.5°	122.8°	−4.2%	4.4%

AMTD
2, 781–824, 2009

Title Page
Abstract | Introduction
Conclusions | References
Tables | Figures
◂ | ▸
Back | Close
Full Screen / Esc
Printer-friendly Version
Interactive Discussion

Table 2. Monthly medians of the ratio of NO_2 measurements performed with photolytic and molybdenum converters at Taenikon, Switzerland, under clear-sky conditions (sunshine fraction of at least 0.8) from 13:00 to 14:00 local time during the period January 1995 to mid-August 2001 (applied for the 7 stations without ozone measurements). The second column shows monthly medians of the correction factors (mean corrected NO_2 divided by mean measured NO_2 for each station) based on regression analysis of the 28 stations with ozone measurements. The relative differences between the two median ratios ((regression ratio-Taenikon ratio)/Taenikon ratio) are also shown.

Month	Median ratio (Taenikon)	Median ratio (Regression)	Relative difference (%)
January	0.850	0.822	−3.3
February	0.774	0.726	−6.3
March	0.667	0.696	4.4
April	0.537	0.653	21.6
May	0.463	0.669	44.6
June	0.488	0.668	36.9
July	0.466	0.722	54.9
August	0.517	0.819	58.4
September	0.647	0.856	32.3
October	0.767	0.866	12.9
November	0.806	0.870	7.9
December	0.873	0.855	−2.1

AMTD

2, 781–824, 2009

Improved tropospheric NO_2 retrieval for satellite observations

Y. Zhou et al.

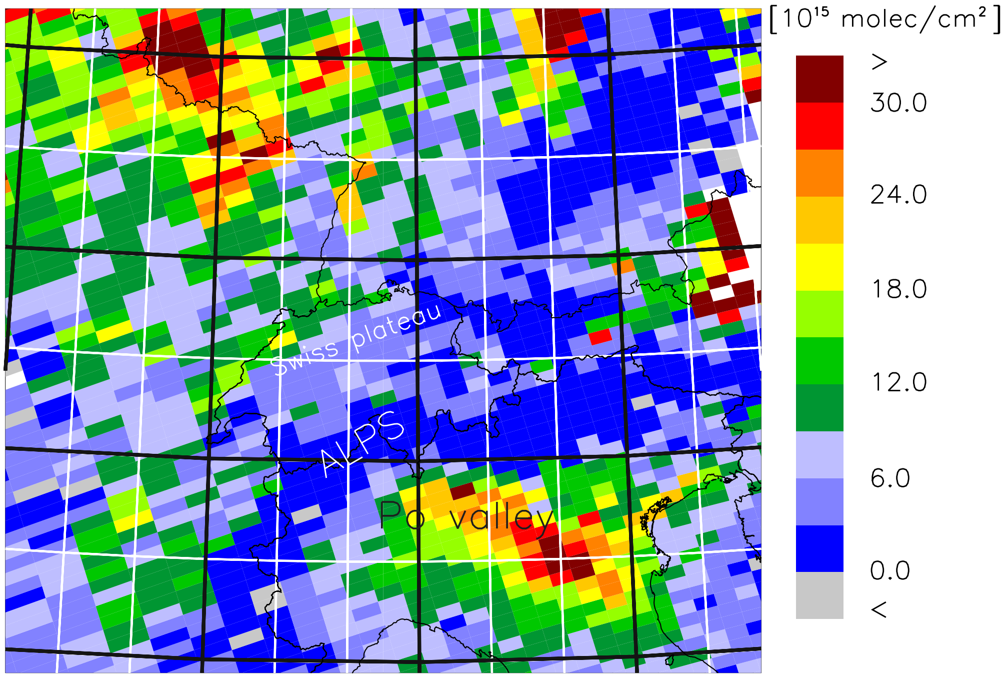

Fig. 1. NO_2 tropospheric vertical columns over central Europe from a single OMI overpass on 3 January 2006. The pixel size varies in across-track direction within the swath, with the highest resolution of about 0.15°×0.2° at nadir. For comparison, the grid of the albedo data set (1°×1°) is overlaid as white lines and the grid of the TM4 chemistry-transport-model (2°×3°) as black lines. The TM4 model (Dentener et al., 2003) determines the resolution of both the a priori profile and the surface pressure, with one grid cell almost as big as Switzerland.

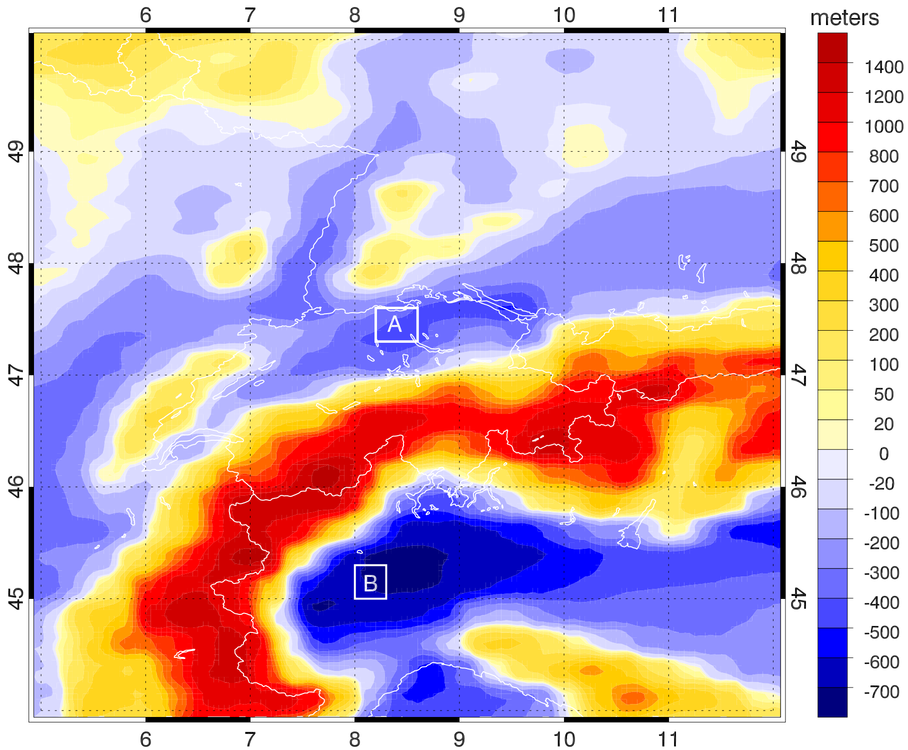

Fig. 2. Difference between effective and TM4 model terrain height ($h_{\text{eff}} - h_{\text{TM4}}$) in meters. Two areas of interest over the Swiss Plateau and the Po Valley in northern Italy referred to in the text are highlighted with labels A (latitude between 47.3° N and 47.6° N, longitude between 8.2° E and 8.6° E) and B (latitude between 45° N and 45.3° N, longitude between 8° E and 8.3° E), respectively.

AMTD

2, 781–824, 2009

Title Page
Abstract
Introduction
Conclusions
References
Tables
Figures
◀◀
▶▶
◀
▶
Back
Close
Full Screen / Esc
Printer-friendly Version
Interactive Discussion

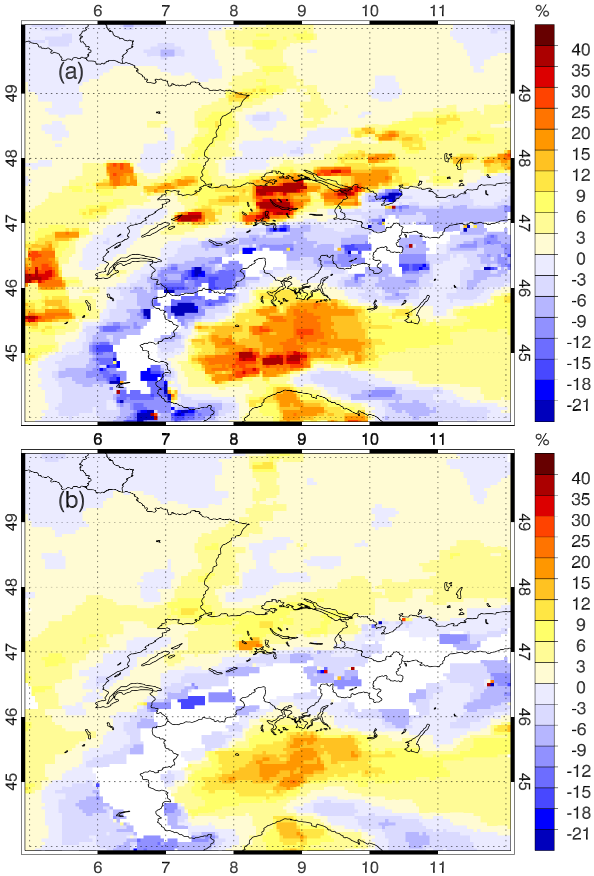

Fig. 3. Relative change in NO_2 VTC retrieved with effective surface pressure p_{eff} instead of TM4 surface pressure p_{TM4} for December 2006. **(a)** Cloud radiance fraction <50% (corresponds to a cloud fraction of only about 20%, and has often been used in previous studies to distinguish between clear and cloudy pixels), **(b)** Cloud radiance fraction <10% (much more stringent than (a) and reduces the data set to virtually cloud-free pixels).

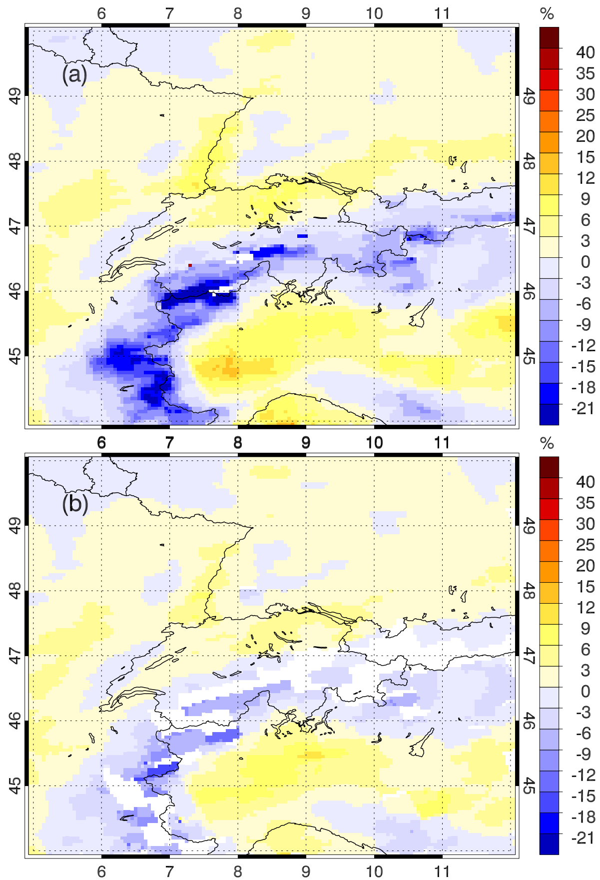

Fig. 4. Same as Fig. 3 but for June 2006. **(a)** Cloud radiance fraction <50%, **(b)** <10%.

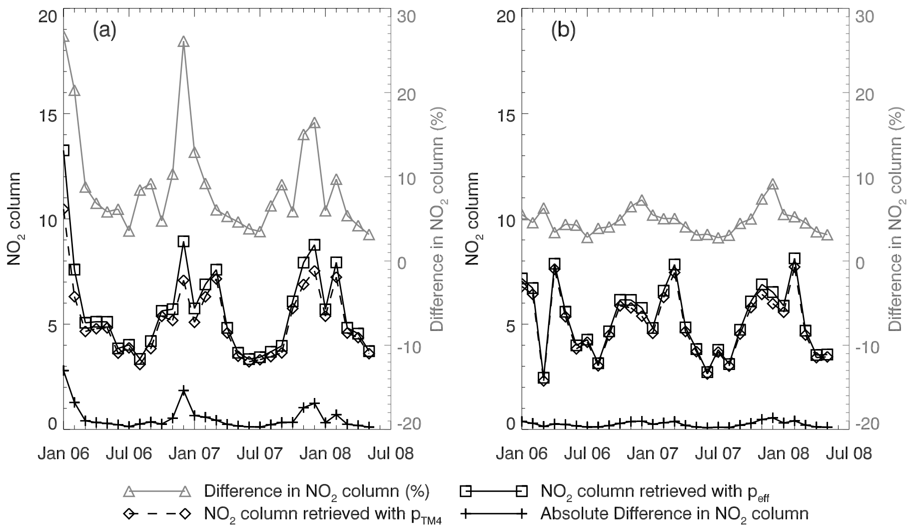

Fig. 5. Seasonal cycles of NO_2 VTC retrieved with effective surface pressure p_{eff} (black solid line with squares) and with TM4 surface pressure p_{TM4} (dashed line with diamonds) in area A over the Swiss Plateau. Also shown are the absolute (black solid line with crosses) and relative differences (grey line, right axis) between the two. **(a)** Cloud radiance fraction <50%, **(b)** <10%.

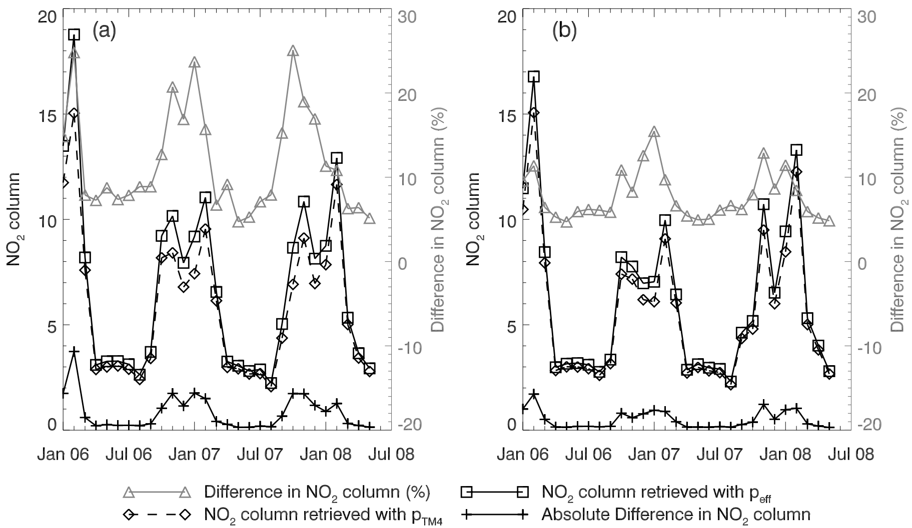

Fig. 6. Same as Fig. 5 but for area B in the Po Valley. **(a)** Cloud radiance <50%, **(b)** <10%.

AMTD
2, 781–824, 2009

Title Page
Abstract
Introduction
Conclusions
References
Tables
Figures
◀
▶
Back
Close
Full Screen / Esc
Printer-friendly Version
Interactive Discussion

AMTD

2, 781–824, 2009

Improved tropospheric NO_2 retrieval for satellite observations

Y. Zhou et al.

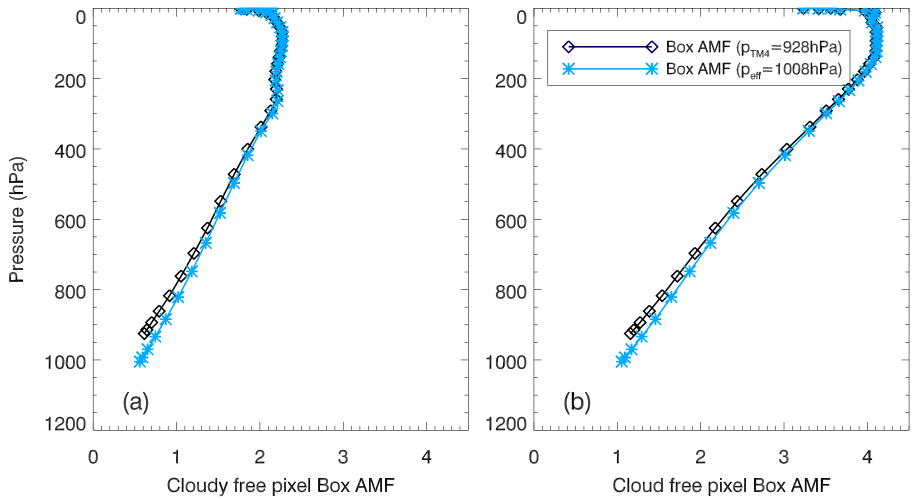

Fig. 7. Profiles of box air mass factors for cloud free pixels in the Po Valley on **(a)** 4 August 2006 (longitude: 8.3°, latitude: 45.14°, albedo=0.057, SZA=31°, AZA=136°, VZA=3°) and **(b)** 1 December 2006 (longitude: 8.22°, latitude: 45.12°, albedo=0.116, SZA=70°, AZA=122.8°, VZA=11.5°). Black lines: For surface pressure p_{TM4}. Blue lines: for effective surface pressure p_{eff}. Each symbol in the curves represents the value at the middle of one of the 34 layers in the TM4 model from the ground to the model top. Due to the hybrid coordinate system, the location of these layers scales with the surface pressure (see Eq. 2).

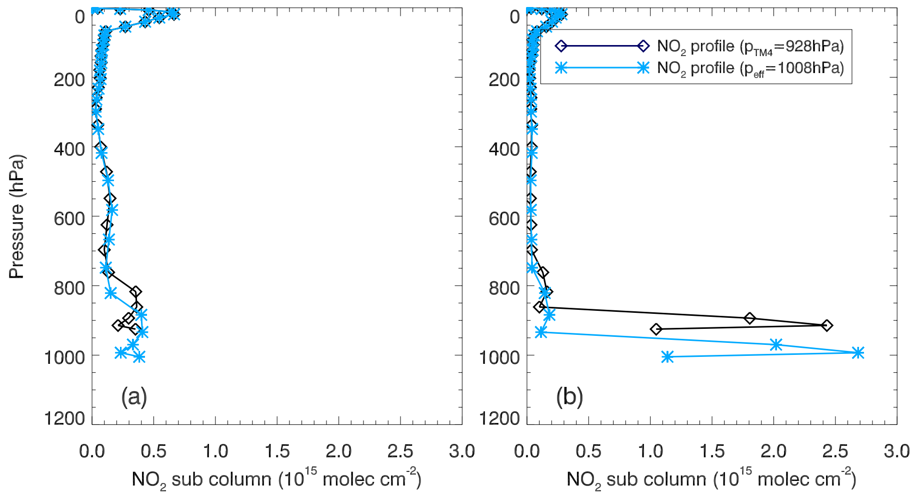

Fig. 8. Same as Fig. 7 but for a priori NO_2 profiles.

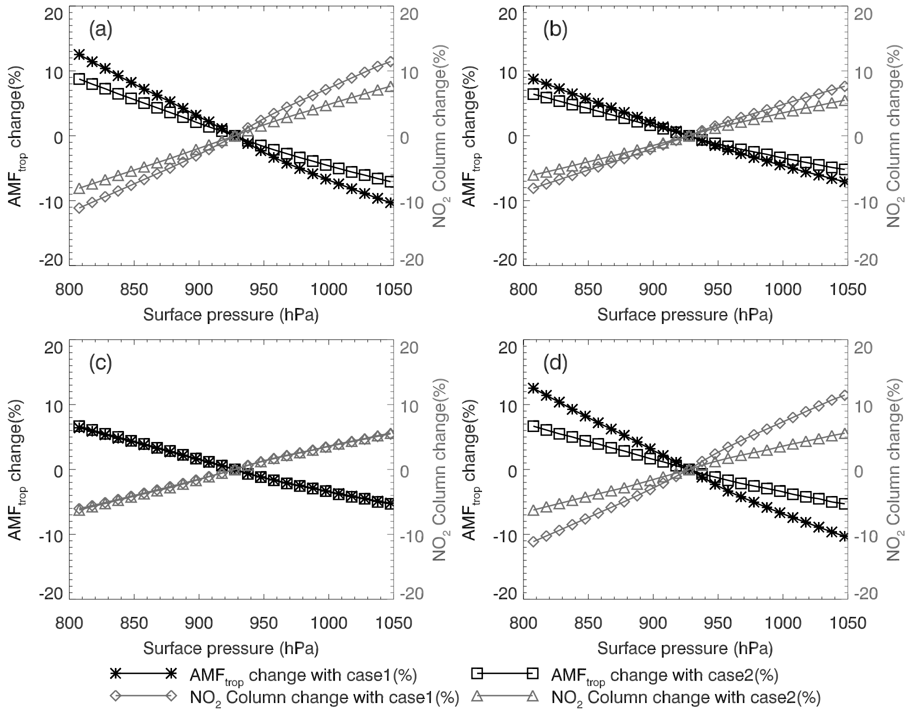

Fig. 9. Effect of different retrieval parameters on the sensitivity of the change in AMF_{trop} (black lines) and NO_2 VTC (grey lines) to a change in surface pressure. The corresponding retrieval parameter settings are listed in Table 1. **(a)** Effect of a priori NO_2 profile (case A1: winter profile, case A2: summer profile), **(b)** solar zenith angle (case B1: SZA=70°, case B2: SZA=31°), **(c)** albedo (case C1: albedo=0.116, case C2: albedo=0.057°), **(d)** combined effect (case D1: winter, case D2: summer).

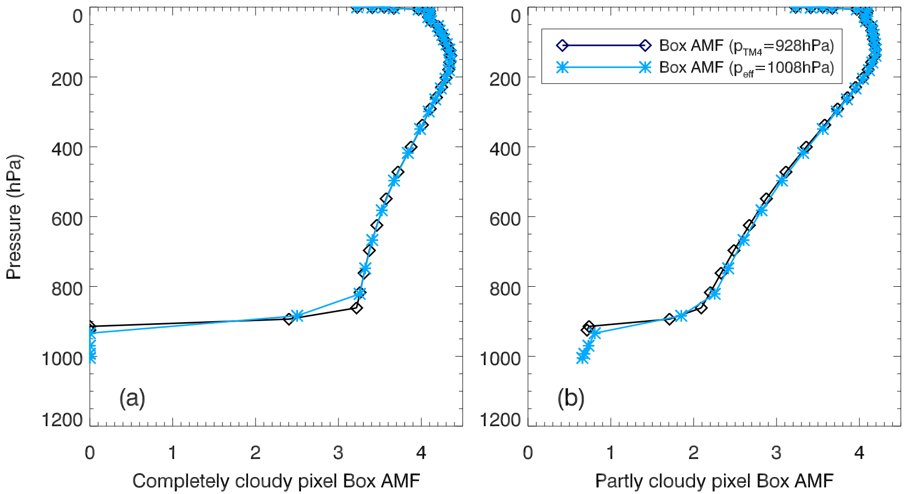

Fig. 10. Profiles of box air mass factors for **(a)** a completely cloudy pixel (cloud albedo=0.8, cloud pressure=900 hPa, SZA=70°, AZA=122.8°, VZA=11.5°) and **(b)** for the same pixel but assumed to be only partly cloudy (surface albedo=0.116, cloud fraction=15%, cloud radiance fraction=38%, cloud pressure=900 hPa). Black lines: For original surface pressure p_{TM4}. Blue lines: for effective surface pressure p_{eff}.

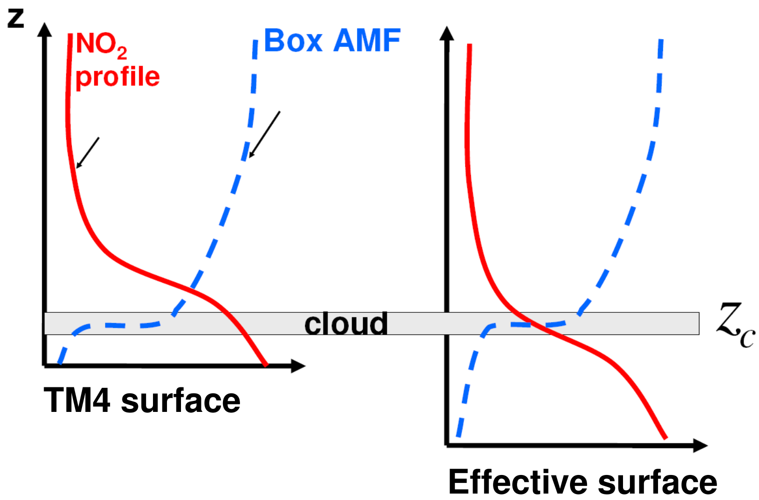

Fig. 11. Illustration of the inaccurate topography effect on partly cloudy pixels. Red lines are the a priori NO_2 profiles, blue dashed lines the box air mass factors. The cloud level remains unchanged when the surface is lowered to the effective altitude in the right hand part of the figure. The a priori NO_2 profile is scaled to the new surface level with all polluted layers now located below cloud top where the sensitivity of the measurement is very low.

AMTD
2, 781–824, 2009

Improved tropospheric NO_2 retrieval for satellite observations

Y. Zhou et al.

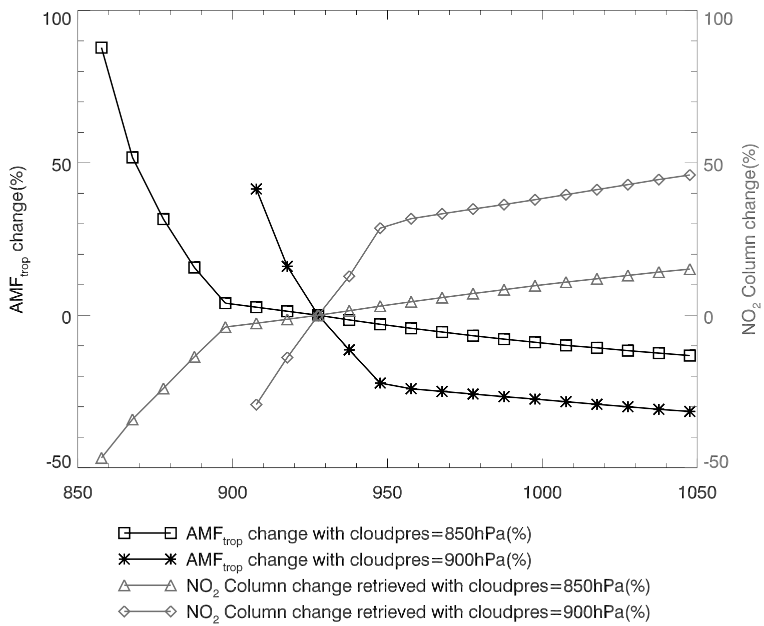

Fig. 12. Effect of cloud pressure on the sensitivity of the change in AMF_{trop} (black lines) and NO_2 VTC (grey lines) to a change in surface pressure (reference point p_{TM4}=928 hPa, cloud fraction=15%).

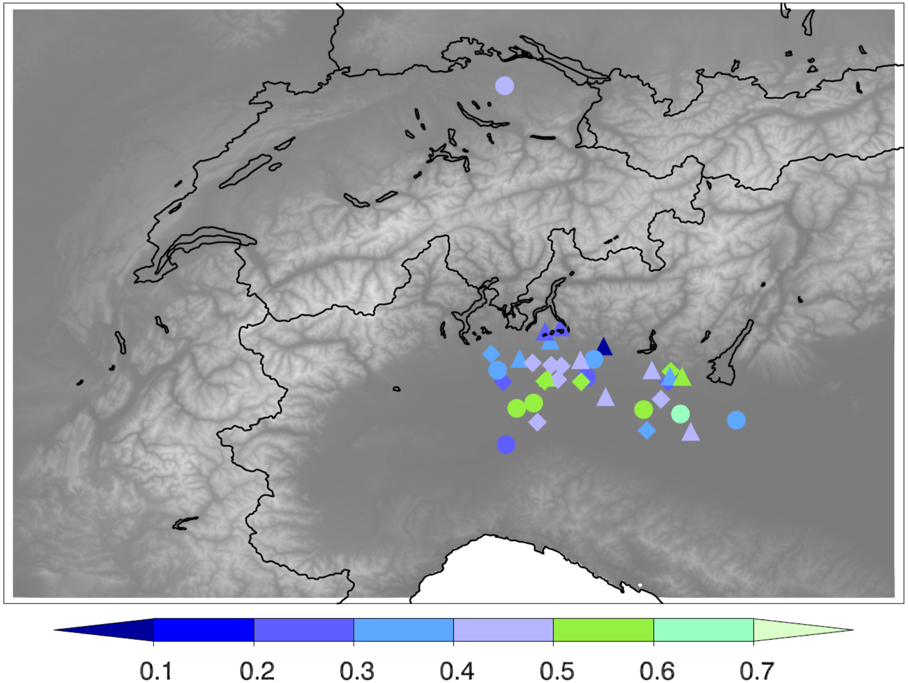

Fig. 13. Topographic map of the Alpine domain with all in situ measurement stations used for validation shown as colored symbols. Colors are correlation coefficients (r^2) between the in-situ and OMI NO_2 VTCs retrieved with effective surface pressure p_{eff} for measurements in 2006 and 2007. Circles represent rural, triangles suburban and diamonds urban stations.

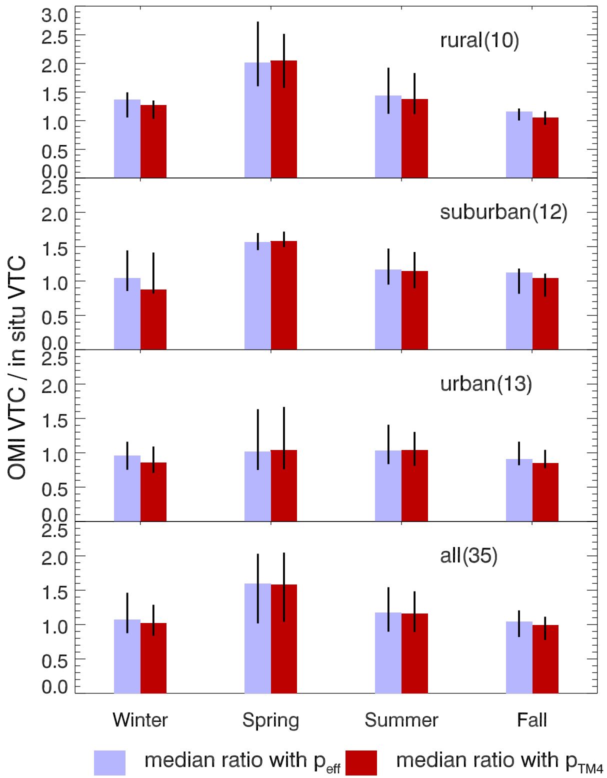

Fig. 14. Medians of the ratios of seasonal mean of OMI NO_2 VTCs and seasonal mean of in-situ NO_2 VTCs (OMI mean divided by in situ mean for each station). The vertical lines depict the central half of the data between the lower ($q_{0.25}$) and the upper quartile ($q_{0.75}$). The measurement sites are classified by land use type as rural, suburban and urban. The number of stations included is given in parentheses.

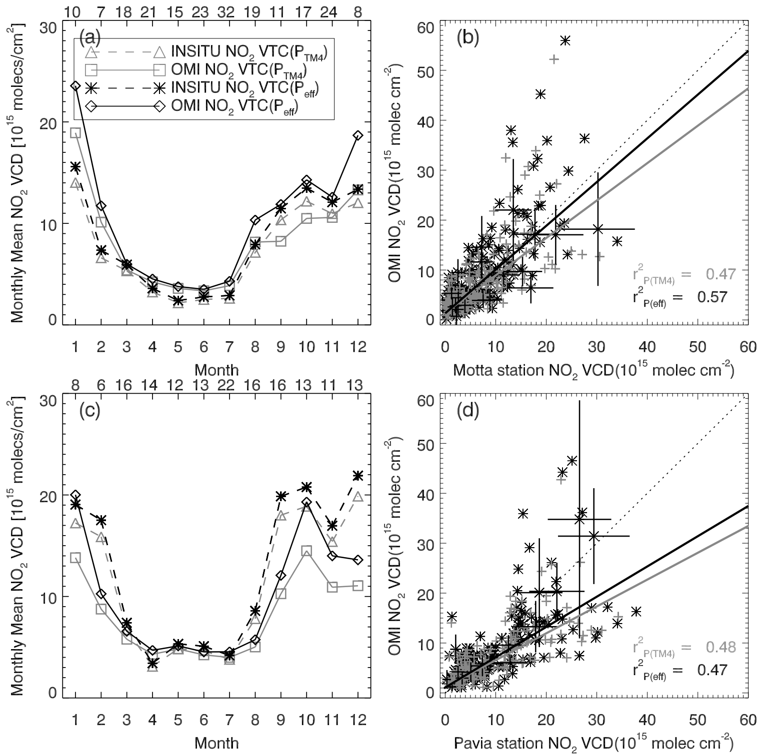

Fig. 15. The left column shows the seasonal cycles of monthly means of in situ and OMI NO_2 VTCs at **(a)** the rural station Motta and **(c)** the urban station Pavia. Numbers above each panel refer to the number of cloud-free (cloud radiance fraction lower than 50%) and snow-free (albedo lower than 0.6) days considered for each month during the two year period 2006–2007. The right column shows the corresponding regression analysis for all individual OMI NO_2 VTCs versus in situ NO_2 VTCs at **(b)** Motta and **(d)** Pavia. Black stars indicate VTCs retrieved with p_{eff}, grey crosses with p_{TM4}. Dotted lines are the 1:1 lines, black and grey solid lines are the weighted orthogonal fits to the data with p_{eff} and p_{TM4}, respectively.